We are IntechOpen, the world's leading publisher of Open Access books
Built by scientists, for scientists

6,900
Open access books available

186,000
International authors and editors

200M
Downloads

Our authors are among the

154
Countries delivered to

TOP 1%
most cited scientists

12.2%
Contributors from top 500 universities

CLARIVATE ANALYTICS
BOOK CITATION INDEX
INDEXED

WEB OF SCIENCE™

Selection of our books indexed in the Book Citation Index in Web of Science™ Core Collection (BKCI)

Interested in publishing with us?
Contact book.department@intechopen.com

Numbers displayed above are based on latest data collected.
For more information visit www.intechopen.com

Chapter 7

Boosting the Amount of Molecular Information Through Polarized Resolved Resonance Raman Scattering

Søren Hassing

Additional information is available at the end of the chapter

http://dx.doi.org/10.5772/65482

Abstract

Vibrational Raman spectroscopy, one of the experimental techniques available, is applied for characterization and analysis of molecular samples in different areas such as medical, food and environmental analysis. Application of the Raman technique is mostly similar to the application of infrared and near-infrared absorption spectroscopy, i.e. only the spectral distribution is analysed. The goal of the present chapter is to demonstrate that the amount of molecular information (also for solutions and powders) can be increased considerably by analysing also the polarization of the Raman and resonance Raman-scattered light. The goal is achieved through: (1) a discussion of the basic properties of Raman scattering with special focus on polarization and polarization dispersion. The discussion includes the rotational invariants of Raman tensors, the non-commuting generator approach to molecular symmetry as a tool for construction of state and Raman tensors for single molecules and dimers and higher aggregates and thereby predict the polarization; (2) a discussion of two illustrative case studies: Case study 1: Aggregation of haemoglobin in red blood cells (RBC); and Case study 2: *In vitro* polarization resolved RRS study of dye-sensitized solar cells.

Keywords: polarization, state tensor, Raman tensor, aggregation, non-commuting generators

1. Introduction

Raman spectroscopy is a fast, non-destructive and molecule-specific technique, which requires no or very little sample preparation. Raman spectroscopy is therefore attractive as an experimental technique for on-site investigations of molecular samples of very different

INTECH
open science | open minds

© 2017 The Author(s). Licensee InTech. This chapter is distributed under the terms of the Creative Commons Attribution License (http://creativecommons.org/licenses/by/3.0), which permits unrestricted use, distribution, and reproduction in any medium, provided the original work is properly cited.

nature. A vibrational Raman spectrum contains the unique and highly resolved vibrational signature of the molecule and it is obtained by illuminating the sample with polarized laser light with wavenumbers in either the near-infrared (NIR), visible or ultraviolet (UV) regions and monitoring the backscattered light as a function of wavenumber. The main challenge of Raman spectroscopy has always been the low Raman cross-section, where typically 10^8 laser photons only generate a single Raman photon. The result is that the intensity in Raman spectra is generally low. Another challenge particular in Raman investigations of biomolecules is that the excitation of the Raman process is followed by a simultaneous excitation of fluorescence. Since the fluorescence cross-section is generally several orders of magnitude higher than the Raman cross-section, the Raman signal may be partly or completely hidden behind the fluorescence background.

However, because of the technical improvements in Raman instrumentation, the problems originating from the low Raman cross-section have largely been overcome so that the potential of Raman scattering can be utilized, and even though fluorescence may still be a problem in some cases and requires advanced signal processing, vibrational Raman spectroscopy is now applied as a standard technique in many areas such as medical, food and environmental analysis.

In most practical applications, only the positions and intensities of the Raman bands are analysed, i.e. the Raman technique is applied similarly to infrared (IR) and NIR spectroscopy. Although the polarization properties of Raman scattering have been known since the early days of Raman theory, see e.g. [1], and although Raman dispersion spectroscopy (including polarization) introduced by Mortensen [2] has been applied for many years to explore conformational perturbations in metallo-porphyrins and various proteins, see [3–7] and references therein, the advantage of applying polarization resolved Raman scattering is not yet common knowledge among the increasing group of practically working scientists and laboratory technicians representing very different areas, who apply vibrational Raman spectroscopy as one out of a large number of experimental techniques available for the characterization of molecular samples. Besides, polarization analysis of vibrational Raman data is not a standard option in most commercial Raman instruments.

A unique property of the Raman process is that the polarization of the scattered light is generally different from the polarization of the incident laser light. This holds for molecular solids, i.e. oriented molecules and (perhaps more surprisingly) also for powders and solutions, where the molecules are randomly oriented. In vibrational Raman scattering, the polarization change is found to be specific for each vibrational Raman mode and for excitations near an UV/Visible absorption in the molecule, i.e. in resonance or near-resonance Raman scattering, the change depends in general on the wavenumber difference between the excitation and the absorption as well as on the molecular configuration in the electronically excited state.

The goal of this chapter is to demonstrate why, how and when the application of polarized resolved Raman spectroscopy may increase the outcome of a Raman experiment. This goal is achieved through a discussion of the basic properties of Raman scattering with special focus on the polarization followed by a discussion of two illustrative case studies: Case study 1:

Aggregation of haemoglobin in red blood cells (RBC); Case study 2: *In vitro* polarization resolved RRS study of dye-sensitized solar cells (DSC).

2. A glimpse of Raman theory

A unified treatment of Raman theory can be found in Ref. [8] together with a long list of references to the Raman literature. The symmetry aspects of the polarization properties have been discussed by Mortensen and Hassing [9], while the vibronic aspects have been discussed by Siebrand and Zgierski [10] and we refer to these references for details.

Raman scattering is a two-photon process in which a primary photon with wavenumber $\tilde{\nu}_p$ and polarization vector $\boldsymbol{u}_p$ is absorbed and coherently replaced by a scattered photon with wavenumber $\tilde{\nu}_s$ and polarization vector $\boldsymbol{u}_s$. In a quantum mechanical description of the process in which the interaction between the molecule and radiation is used as perturbation, the Raman process is of second-order, which has the consequence that the Raman-scattered intensity into the solid angle $d\Omega(I_{\text{Raman}})$ becomes proportional to the absolute square of the scattering (Raman) tensor $|\boldsymbol{\alpha}^{a\to b}|^2$ which is a tensor of Rank 2. The basic scattering equations are collected in Eq. (1), while the expression for the components of the Raman tensor $\boldsymbol{\alpha}_{\varrho\sigma}^{a\to b}$ is given in Eq. (2).

$$I_{\text{Raman}} = \left(\frac{d\sigma}{d\Omega}\right) I_{\text{laser}}\, d\Omega \text{ and } \left(\frac{d\sigma}{d\Omega}\right) = 4\pi\, \boldsymbol{\alpha}_{\text{fsc}}^2\ \tilde{\nu}_s^4 \left| \sum_{\rho,\sigma} u_{s\rho}\, \boldsymbol{\alpha}_{\varrho\sigma}^{a\to b}\, u_{p\sigma} \right|^2 \tag{1}$$

where $\left(\frac{d\sigma}{d\Omega}\right)$ is the differential Raman cross-section and α_{fsc} is the fine structure constant. I_{laser} is the intensity of a collimated laser beam:

$$\boldsymbol{\alpha}_{\varrho\sigma}^{a\to b} = \sum_r \frac{\langle \boldsymbol{b}|\rho|r\rangle\langle r|\sigma|\boldsymbol{a}\rangle}{\tilde{\nu}_{pa} - \tilde{\nu}_p - i\,\gamma_r} + \frac{\langle \boldsymbol{b}|\sigma|r\rangle\,\langle r|\rho|\boldsymbol{a}\rangle}{\tilde{\nu}_{rb} + \tilde{\nu}_p + i\,\gamma_r} \tag{2}$$

where a, b and r stands for the initial, final and intermediate states of the process. $\tilde{\nu}_{ra}$ is the energy difference between state $|r\rangle$ and $|\boldsymbol{a}\rangle$ The summation runs over all the (exact) eigenstates of the molecule and γ_r is the damping of the state $|r\rangle$ responsible for its exponential decay. ρ and ρ and σ are a shorthand notation for the Cartesian components of the electronic position vector $\sum_i r_i = \frac{\hat{\mu}}{e}$, where $\hat{\mu}$ and e are the electric dipole operator of the electrons and the electron charge, respectively, and the summation runs over all electrons in the molecule. ρ and σ refer either to the space-fixed coordinates X, Y,Z or to the molecule-fixed coordinates x, y, z. In non-resonance Raman scattering (RS), where the excitation wavenumber is chosen in a region, where the molecule does not absorb light, i.e. $\tilde{\nu}_b < \tilde{\nu}_p \ll \tilde{\nu}_{ra}$ for any state $|r\rangle$, the expression for $\boldsymbol{\alpha}_{\varrho\sigma}^{a\to b}$ becomes virtually independent of intermediate states and the polarizability theory first developed by Placzek applies [1]. See also the book by Long [11]. In the case of excitation close to an absorption energy, i.e. $\tilde{\nu}_p \sim \tilde{\nu}_{ra}$ for some intermediate states, the contribution from these states dominates and the Raman signal will be enhanced. The process is termed resonance Raman scattering (RRS). The enhancement, which may be a factor of 10^6, depends on the wavenumber difference between the resonating states $|r\rangle$ and the wavenumber of the laser $\tilde{\nu}_p$ as well as on the magnitude of the damping constants γ_r.

In polarization resolved Raman scattering two quantities are measured, the parallel and perpendicular components of the total scattering cross-section,

$$\left(\frac{d\sigma}{d\Omega}\right)_{\parallel} = 4\pi\, \boldsymbol{\alpha}_{\text{fsc}}^{2}\ \ \tilde{\nu}_{s}^{4}\ \left|\alpha_{ZZ}^{a\to b}\right|^{2} \tag{3}$$

$$\left(\frac{d\sigma}{d\Omega}\right)_{\perp} = 4\pi\, \boldsymbol{\alpha}_{\text{fsc}}^{2}\ \ \tilde{\nu}_{s}^{4}\ \left|\boldsymbol{\alpha}_{YZ}^{a\to b}\right|^{2} \tag{4}$$

$$DPR = \frac{\left(\frac{d\sigma}{d\Omega}\right)_{\perp}}{\left(\frac{d\sigma}{d\Omega}\right)_{\parallel}} = \frac{\left|\boldsymbol{\alpha}_{YZ}^{a\to b}\right|^{2}}{\left|\boldsymbol{\alpha}_{ZZ}^{a\to b}\right|^{2}} \tag{5}$$

where it is assumed that an oriented molecule is placed in the centre of a space-fixed coordinate system and that the Raman scattering is observed in the backscattering geometry. Besides the incoming light is taken to propagate along the X-axis and linearly polarized in the Z-direction. The parallel polarized scattered light is then also polarized in the Z-direction, while the perpendicular polarized scattered light is polarized in the Y-direction. The polarization is described by the depolarization ratio (DPR) defined in Eq. (5). The DPR is seen to be an absolute quantity.

For ensembles of randomly oriented molecules, i.e. powders and solutions, the parallel and perpendicular scattering cross-sections in Eqs. (3) and (4) must be averaged with respect to molecular orientation. The spatial average of the scattering components $\langle \left|\boldsymbol{\alpha}_{ZZ}^{a\to b}\right|^{2} \rangle$ and $\langle \left|\boldsymbol{\alpha}_{YZ}^{a\to b}\right|^{2} \rangle$ have been evaluated by Mortensen and Hassing by applying angular momentum theory [9]. The result is that $\langle \left|\boldsymbol{\alpha}_{ZZ}^{a\to b}\right|^{2} \rangle$ and $\langle \left|\boldsymbol{\alpha}_{YZ}^{a\to b}\right|^{2} \rangle$ are expressed in terms of the three rotational invariants of the Raman tensor Σ^0, Σ^1 and Σ^2, which contain combinations of the absolute squares of the tensor components. Σ^0 is the absolute square of the trace of Raman tensor and Σ^2 contains symmetric combinations of the off-diagonal tensor components and diagonal components and is termed the symmetric anisotropy. Σ^1 only contains anti-symmetric combinations of the tensor components, i.e. $\left|\boldsymbol{\alpha}_{\rho\sigma}^{a\to b} - \boldsymbol{\alpha}_{\sigma\rho}^{a\to b}\right|^{2}$. The complete relations between the invariants and the Raman tensor components are given in Ref. [9].

For randomly oriented systems Eqs. (3)–(5) must be then replaced by,

$$\left(\frac{d\sigma}{d\Omega}\right)_{\parallel} = 4\pi\, \boldsymbol{\alpha}_{\text{fsc}}^{2}\ \ \tilde{\nu}_{s}^{4}\, \frac{1}{15}(5\,\Sigma^{0} + 2\,\Sigma^{2}) \tag{6}$$

$$\left(\frac{d\sigma}{d\Omega}\right)_{\perp} = 4\pi\, \boldsymbol{\alpha}_{\text{fsc}}^{2}\ \ \tilde{\nu}_{s}^{4}\, \frac{1}{15}\left(\frac{3}{2}\,\Sigma^{2} + \frac{5}{2}\,\Sigma^{1}\right) \tag{7}$$

$$DPR = \frac{\left(\frac{d\sigma}{d\Omega}\right)_{\perp}}{\left(\frac{d\sigma}{d\Omega}\right)_{\parallel}} = \frac{3\,\Sigma^{2} + 5\,\Sigma^{1}}{10\,\Sigma^{0} + 4\,\Sigma^{2}} \tag{8}$$

First, it is noted that in RRS all three tensor invariants may be different from zero, while in RS the Raman tensor is found to be symmetric so that the scattering is determined by only Σ^0 and Σ^2, which has the consequence is that the DPR is limited to: $0 \le DPR \le \frac{3}{4}$. However, in RRS the DPR may take any number. But more important: the DPR may depend on the laser wavenumber, i.e. exhibit polarization dispersion.

We now see why polarized measurements performed on powders and solutions may provide extra information in Raman spectroscopy, while this is not the case in IR and NIR absorption.

http://dx.doi.org/10.5772/65482

Raman scattering includes in general three independent observables $\sum^0$, $\sum^1$ and $\sum^2$ while IR and NIR absorption only includes one observable, namely the spatially average of the electric dipole transition moment vector, i.e. its length. Polarized measurements in IR and NIR absorption may of course give additional information when the molecules can be spatially oriented.

2.1. State tensors and Raman tensors

In the discussion of the polarization properties of RRS, it is convenient to define for the state $|r\rangle$ the state tensor $\left[S_{\varrho\sigma}^{|r\rangle}\right]_{a\to b} = \langle b|\varrho|r\rangle\langle r|\sigma|a\rangle$. The Raman tensor for the Raman transition $|a\rangle \to |b\rangle$ is then given as a sum of state tensors, where each state tensor is weighted by the complex energy factor $\left(\widetilde{\nu}_{ra} - \widetilde{\nu}_p - i\gamma_r\right)^{-1}$. In the general case where the molecule has no symmetry all components of the state tensors $\left[S_{\varrho\sigma}^{|r\rangle}\right]_{a\to b}$ may be different, besides the state tensors $\left[S_{\varrho\sigma}^{|r\rangle}\right]_{a\to b}$ and $\left[S_{\varrho\sigma}^{|r\rangle}\right]_{a\to b}$ associated with different states $|r\rangle$ and $|s\rangle$ are also different in general. When the molecules have a certain amount of symmetry some of the components $\left[S_{\varrho\sigma}^{|r\rangle}\right]_{a\to b}$ vanish and some of the non-vanishing components become numerically related. However, the symmetry relations between the state tensor components $\left[S_{\varrho\sigma}^{|r\rangle}\right]_{a\to b}$ and $\left[S_{\varrho\sigma}^{|r\rangle}\right]_{a\to b}$ may still be different, depending on the symmetry relation between the states $|r\rangle$ and $|s\rangle$. The result is that a particular tensor component $\alpha_{\varrho\sigma}^{a\to b}$ of the Raman tensor $\alpha^{a\to b}$ will have contributions from selected states $|r\rangle$, while other components $\alpha_{\varrho'\sigma'}^{a\to b}$ will have contributions from other states $|s\rangle$. The important point is that the distribution of the state tensor components that contribute to a given Raman tensor $\alpha^{a\to b}$ will manifest itself in the measured DPR values. Thus, under-resonance or near-resonance excitations the value of the DPR may or may not depend on the excitation wavenumber (polarization dispersion). As already mentioned polarization dispersion has been applied in numerous resonance Raman studies of the structure and bio-functionality of proteins containing metallo-porphyrins [7, 12]. The ideal symmetry of the porphyrin (e.g. the haem group) is D_{4h}, but the real symmetry becomes lower when distortions are induced on the Tetra-pyrrole ring by its surroundings. Depending on the symmetry of the distortion the coupling between the doubly degenerate *B*- and *Q*-states of the chromophore induces changes in the state and Raman tensors, which give rise to a characteristic polarization dispersion of each Raman mode. Since the DPR is very sensitive to even small perturbations of the molecule, detailed information about intra-molecular interactions can be obtained as shown in the papers mentioned above. The challenge in performing Raman dispersion studies is that one has to monitor two Raman cross-sections, $\left(\frac{d\sigma}{d\Omega}\right)_{\parallel}$ and $\left(\frac{d\sigma}{d\Omega}\right)_{\perp}$ as a function of excitation wavenumber, which requires special laser sources and/or several lasers. The experiments may be rather time consuming as such, in particular when the fluorescence background changes with the excitation wavenumber. Besides, one has to keep track on the absolute intensity variations by the application of internal standards.

In non-resonance, vibrational Raman scattering the different contributions to the Raman tensor are 'washed out' and the Raman tensor becomes symmetric and as well known, the DPR values become either $DPR_{\text{asym}} = \frac{3}{4}$ for a-symmetric modes or $0 \le DPR_{\text{sym}} < \frac{3}{4}$ for totally symmetric modes.

For molecules with a well-defined nuclear configuration, the molecular symmetry can be discussed in terms of point-groups. As shown by Mortensen and Hassing [9], the general form of

the state tensors, determined by symmetry, can be evaluated by applying the method of non-commuting generators instead of conventional group representation theory [13]. The state tensors for almost all point groups have been derived in [9] and they have later been reproduced in [8]. Below it is demonstrated how this method can be extended to derive also the state tensors for aggregated molecules. Although the dimer is used as an illustrative example the method can easily be generalized to larger aggregates.

Finally, most treatments of vibrational Raman scattering are formulated within the adiabatic Born-Oppenheimer (ABO) approximation and we shall also do so here, since this will be sufficient for the discussion of the polarization. In any case, the results can be generalized to go beyond the ABO approximation by the application of perturbation theory. However, all results based on symmetry will be exact. Since we are mainly interested in larger molecules, i.e. solutions and powders, the rotational motion need not be explicitly considered. All states in the state and Raman tensors are therefore given as products of an electronic state and a vibrational sub-state, i.e. $|r\rangle = |e\rangle|v_1, v_2, v_3, \ldots\rangle$, where in the harmonic approximation the vibrational sub-states are also factorized.

2.2. State and Raman tensors for aggregated molecules

The non-commuting generator approach to molecular symmetry discussed by Mortensen in [13] is illustrated in **Figure 1**, using the point group D_4 as an example. The group is characterized by two generators $\widehat{C}_4$ and $\widehat{C}_{2y}$ and a commutation relation between the generators. The character table, used in group representation theory (shown to the right), is replaced by an eigenvalue table containing the eigenvalues of the generators (region I). Region II gives the eigenvalues under $\widehat{C}_{2y}$, but since this operator does not always commute with $\widehat{C}_4$ the transformation matrix showing how the two basis states $|E_x\rangle$ and $|E_y\rangle$ transform into each other is given instead. Notice that this is the particular information missing in group representation theory since only the characters (i.e. the traces) of the transformation matrices representing the symmetry operators are determined. It follows from **Figure 1** that the trace for both generators for the degenerate *E*-representation is equal to zero in accordance with the value in the character table.

The main task of symmetry is to calculate matrix elements or rather to point out the particular matrix elements that must vanish because of symmetry. The calculation of matrix elements and derivation of symmetry relations between matrix elements, using the non-commuting generator approach, is summarized in **Figure 2**.

In **Figure 2**, the possibility (I) is applied to derive spectroscopic selection rules, while possibility (II) is the one that can be applied to find numerical relations between matrix elements and to derive the general form of the state tensors and the Raman tensors for single molecules. The numerical relations between matrix elements are found by combining (I) and (II) and applying the Wigner Eckart theorem, see Ref. [13].

The state tensors obtained for a molecule with D_{4h} -symmetry, is given in the upper part of **Figure 4** for the Raman modes b_{1g}, b_{2g} and a_{2g} as examples. This applies to the haem, when assuming its ideal symmetry to be D_{4h}. The symmetry of the Raman mode is given in front of each tensor, while the symmetry inside the tensors is the symmetry of the electronic state, i.e. $|E_{Qx}\rangle$ or $|E_{Qy}\rangle$ responsible for that particular tensor component. The state tensors associated

http://dx.doi.org/10.5772/65482

A review of the non-commuting generator approach to molecular symmetry

The principles of the method in brief:

- Generators of the group and commutation relations
- Eigenvalue tables versus character tables, e.g. D_4.

Eigenvalue table

		$\lambda(\hat{C}_4)$	$\lambda(\hat{C}_{2y})$
I	A_1	1	1
	A_2	1	-1
	B_1	-1	1
	B_2	-1	-1
II	E_x	$\begin{pmatrix} 0 & -1 \\ 1 & 0 \end{pmatrix}$	-1
	E_y		1

Real basis

Character table

D_4	E	$2C_4$	C_2	$2C_2'$	$2C_2''$
A_1	1	1	1	1	1
A_2	1	1	1	-1	-1
B_1	1	-1	1	1	-1
B_2	1	-1	1	-1	1
E	2	0	-2	0	0

Generators in D_4: $\hat{R} = \hat{C}_4, \hat{C}_{2y}$

Commutation relation: $\hat{C}_{2y}\hat{C}_4 = \hat{C}_4^{-1}\hat{C}_{2y}$

Eigenvalues: $\lambda(\hat{R}) = e^{i\frac{2\pi}{n}k}$, k = 0, 1, 2, … n-1, (n = group order)

UNIVERSITY OF SOUTHERN DENMARK.DK

Figure 1. Eigenvalue table and character table for point group D_4. Group generators and their commutation relation are given.

Calculation of matrix elements by application of the non-commuting generator approach

Basic selection rule: $\hat{R}\langle b|\hat{O}|a\rangle = \langle b|\hat{O}|a\rangle$ (1)

for $\hat{R}$ equal to each group generator.

Possibility (I):

When the operator $\hat{O}$ and the states ⟨b| and |a⟩ **all** have eigenvalues under $\hat{R}$, application of (1) gives: $\lambda_b(\hat{R}) = \lambda_{\hat{O}}(\hat{R}) \cdot \lambda_a(\hat{R})$ (2)

Possibility (II):

When instead $\hat{O}$, ⟨b| and |a⟩ transform into other operators/states, then application of (1) gives rise to numerical relations between matrix elements.

These relations can be extracted from the eigenvalue tables.

Thus, the non-commuting generator approach may give additional information compared to conventional representation theory.

UNIVERSITY OF SOUTHERN DENMARK.DK

Figure 2. Calculation of symmetry based relations between matrix elements through the application of non-commuting generator approach [13].

with the vibrational sub-states are found by taking the direct product of the symmetry of the electronic state and the symmetry of the Raman mode. Having calculated the distribution of state tensors the Raman tensors and the invariants can be calculated and finally the DPR is calculated from Eq. (8). The DPR values are listed behind the state tensors. Notice that due the high symmetry no polarization dispersion occurs.

When the configuration of the haem is perturbed so that the symmetry becomes lower than D_{4h} the energy of $|E_{Qx}\rangle, |E_{Qy}\rangle$ and of the next excited states $|E_{Bx}\rangle, |E_{By}\rangle$ (Soret absorption band) split up due to coupling induced by the perturbations. As shown by Siebrand and Zgierski [10] and Schweitzer Stenner et al. [14] this will give rise to a mixing of the Raman tensors for different modes and result in characteristic polarization dispersion curves for most Raman modes, from which detailed information about the symmetry lowering perturbations can be extracted. We shall not consider these cases further, but refer to the papers just mentioned. Instead we consider the construction of state and Raman tensors for molecular aggregates using the non-commuting generator approach. The molecular dimer of two coupled haem-groups is chosen as an illustrative case. For simplicity only the excitonic coupling between the $|E_{Qx}\rangle, |E_{Qy}\rangle$-states is considered.

The construction of the state tensors for the molecular dimer by the application of the non-commuting generator approach consists of three steps, which are summarized in **Figure 3**.

In step 1, the coupling matrix describing the electronic coupling between the Q-states of the monomers is defined. Considering, e.g. a H-type dimer the elements in the coupling matrix are $h_{xx} = h_{yy} \equiv h_e$ and $h_{xy} = h_{yx} \equiv h'_e$.

In step 2, the eigenstates and eigenvalues are determined by diagonalisation of the coupling matrix. Finally, in step 3 the state tensors of the dimer in the basis of the monomers are evaluated by inserting the eigenstates and the components of the dipole moment operator of the dimer and applying the symmetry relations between the tensor elements of the monomers.

The state tensors obtained for the H-type dimer for the Raman modes b_{1g}, b_{2g} and b_{1g}, b_{2g} and a_{2g} is shown **Figure 4(b)**. From the state tensor patterns the Raman tensors can then be evaluated by adopting the Franck-Condon principle for the symmetric modes and the general vibronic relation $S_{Q\sigma}^{|e,0\rangle} = S_{\sigma Q}^{|e,1\rangle}$ for the asymmetric modes.

The following should be noticed from **Figure 4**: (1) only 2 of the 4 basis states termed $|R_1\rangle$ and $|R_2\rangle$ contribute to the scattering. (2) The state tensors contain 4 elements instead of 2 as for the monomers. (3) The numerical relations between these tensor elements depend on the symmetry of the Raman mode. (4) The energy factors depends linearly on the coupling parameters h_e and h_e and h'_e. Because of the changed state tensor pattern of the dimer as compared to the monomers, changes are introduced in the Raman tensors with the consequence that the DPR now exhibit polarization dispersion. A similar calculation can be made for J-type dimer as well. The simulated polarization dispersion curves of H-type and J-type

dimers of molecules with D_{4h} symmetry shown in **Figure 5(b)** demonstrate that it is possible to determine the kind of dimerization by polarized resolved RRS.

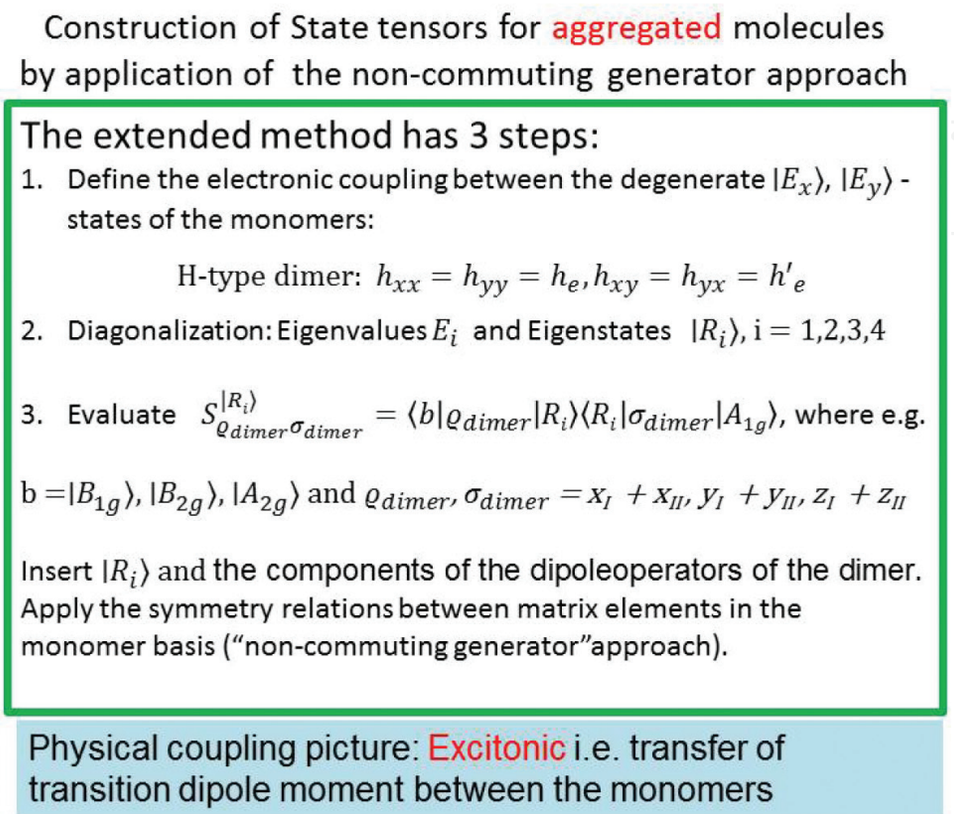

Figure 3. Construction of state tensors for excitonic coupled molecules illustrated by an H-type dimer.

In Ref. [15], a discussion based on a physical and vibronic model of polarization dispersion in H-type and J-type dimers is presented and it is concluded that polarization resolved RRS (i.e. DPR) appears to be a powerful tool for determining the geometries and coupling strengths for molecular dimers and larger aggregates.

2.2.1. Case study 1: aggregation of haemoglobin in red blood cells

Aggregation of biomolecules plays an important role in various biophysical processes, e.g. oxygen uptake, processes involving drug uptake by human cells [16, 17]. In nature many of these important biophysical processes are dependent upon various minor changes of the molecular configurations as well as on various aggregation processes of the biomolecules involved. As already mentioned an important class of biomolecules is the metallo-porphyrins, where extensive systematic studies applying polarized Raman dispersion spectroscopy and including vibronic theory as well as experiments, have been performed [4, 6, 7, 12, 14, 18–22].

Theoretical quantum computations, e.g. density functional theory (DFT), and normal coordinate structural decomposition (NSD) have also been applied [23–26]. The oxidation state of haemoglobin in a single red blood cell (RBC) has been studied *in vivo* applying RRS with different excitation wavelengths by Wood and McNaughton [27], while Ramser et al. have demonstrated that single RBC's can be studied by trapping the cell with optical tweezers [28].

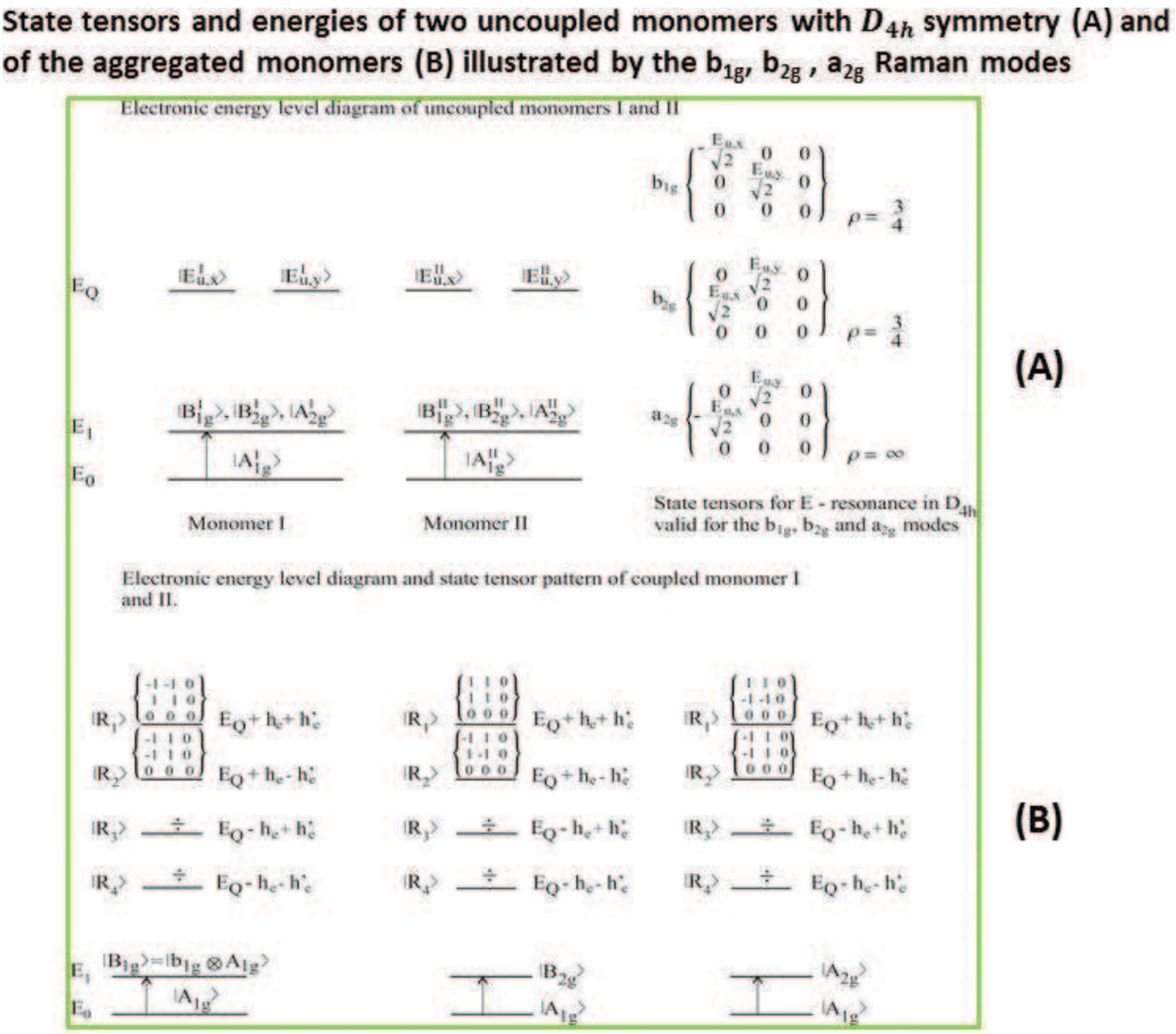

Figure 4. Energy level scheme and state tensors for uncoupled monomers and for the H-type dimer. Monomers: the symmetry written in the tensor means that the number in that position is due to a state with that symmetry, while the signs show the quantitative relation between the tensor elements. Dimer: The numerical relations between the tensor elements are indicated with ±1. The Wigner-Eckart theorem has been applied.

In the following the aggregation of haemoglobin molecules in living RBC's of human blood is discussed. First, the polarized resolved Raman study on spatially oriented RBCs performed by Wood et al. in Ref. [29] is discussed. The coordinates, which constitutes the laboratory frame, are designated ⊥ and ∥ and for the molecular frame these are designated *X*, *Y*, *Z*. The erythrocytes were affixed in a horizontal and vertical direction relative to a petri dish surface. In the horizontal situation the Petri dish surface is parallel to the ⊥, ∥ –plane, while in the vertical situation it is perpendicular to this plane. The polarization of the laser is directed

http://dx.doi.org/10.5772/65482

along ∥-axis and is, besides, identical in the two situations. Subsequently 30 Raman spectra were measured in each situation, where in each case both the parallel and perpendicular polarization of the scattering were measured. The polarized Raman experiment may now be described by the following equations,

$$\left(\frac{d\sigma}{d\Omega}\right)_{\parallel}^{(1)} = 4\pi\,\alpha_{\mathrm{fsc}}^{2}\;\tilde{\nu}_{s}^{\,4}\left|\alpha_{ZZ}^{\mathrm{RBC}}\right|^{2}\;;\;\left(\frac{d\sigma}{d\Omega}\right)_{\perp}^{(1)} = 4\pi\,\alpha_{\mathrm{fsc}}^{2}\;\tilde{\nu}_{s}^{\,4}\left|\alpha_{XZ}^{\mathrm{RBC}}\right|^{2} \tag{9}$$

$$DP\,R_{1}^{\mathrm{RBC}} = \frac{\left|\alpha_{XZ}^{\mathrm{RBC}}\right|^{2}}{\left|\alpha_{ZZ}^{\mathrm{RBC}}\right|^{2}} \tag{10}$$

$$\left(\frac{d\sigma}{d\Omega}\right)_{\parallel}^{(2)} = 4\pi\,\alpha_{\mathrm{fsc}}^{2}\;\tilde{\nu}_{s}^{\,4}\left|\alpha_{ZZ}^{\mathrm{RBC}}\right|^{2}\;;\;\left(\frac{d\sigma}{d\Omega}\right)_{\perp}^{(2)} = 4\pi\,\alpha_{\mathrm{fsc}}^{2}\;\tilde{\nu}_{s}^{\,4}\left|\alpha_{YZ}^{\mathrm{RBC}}\right|^{2} \tag{11}$$

$$DP\,R_{2}^{\mathrm{RBC}} = \frac{\left|\alpha_{YZ}^{\mathrm{RBC}}\right|^{2}}{\left|\alpha_{ZZ}^{\mathrm{RBC}}\right|^{2}} \tag{12}$$

The philosophy behind the polarized Raman experiments performed with the spatially oriented RBC's in [29] is that if no aggregation between the haemoglobin molecules takes place inside the RBCs, then $DP\,R_{1}^{\mathrm{RBC}} \approx DP\,R_{2}^{\mathrm{RBC}}$, whereas if an aggregation takes place $DP\,R_{1}^{\mathrm{RBC}} \neq DP\,R_{2}^{\mathrm{RBC}}$. The parallel polarized spectra of the horizontally and the vertically oriented RBCs were compared by applying a principal component analysis (PCA) to the data. The same analysis was performed for the perpendicular polarized spectra. Since the PCA performed on both sets of data containing the polarization parameter showed significantly different results, it was concluded that a distinct ordering of the haemoglobin took place in the erythrocytes.

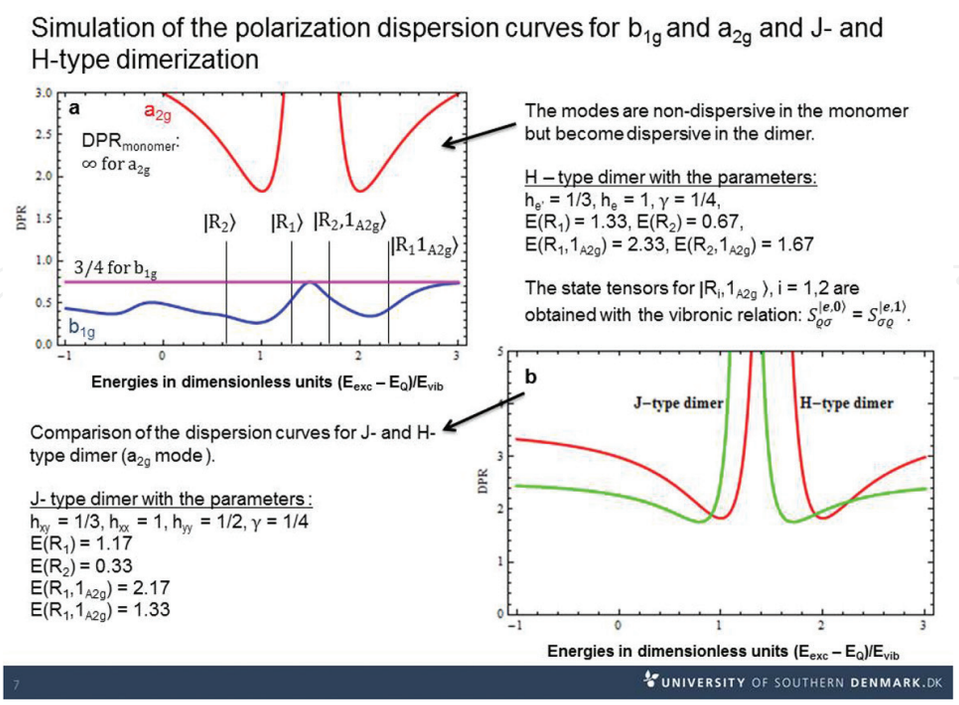

Figure 5. Simulated polarization dispersion curves for dimers. (a) Illustrates that non-dispersive modes become dispersive due to aggregation. (b) Demonstrates that it is possible to distinguish between J-type and H-type dimerization by polarization resolved RRS.

It is important, when studying the properties of biomolecules and biophysical processes, to mimic the natural surrounding conditions. When for example carrying out Raman studies of the aggregation process of haemoglobin in RBCs, this means that it is preferable to perform the polarization resolved measurements directly on a solution of the RBCs and thereby avoiding the consequences of a molecular fixation used by Ramser et al. [28] and by Wood et al. [29]. The basis for such an investigation is the results expressed in Eqs. (6)–(8). In our measurements the procedure was as follows: First, the polarized resolved RRS spectra were measured on a sample containing a number of randomly oriented erythrocytes (i.e. a dilute solution where no aggregation between the RBCs occurs). Secondly, the polarized resolved RRS spectra were measured of a reference sample containing a number of randomly oriented haemoglobin molecules (i.e. a dilute solution where no aggregation occurs). After inspection of the visible absorption spectra of selected haem-proteins, measured in [30], the excitation was chosen as 532 nm, which corresponds to resonance with the vibronic part of the *Q*-band. The DPR values obtained from the most intense Raman modes in the two cases were then compared. As opposed to the experiments with the oriented/fixed RBCs in [29] our results shown in **Figure 6**, demonstrate that the application of PCA is unnecessary when proving the aggregation of haemoglobin, since the changes in the DPR of most Raman active modes are large. In particular, the DPR of the inversely polarized a_{2g} modes exhibits large changes.

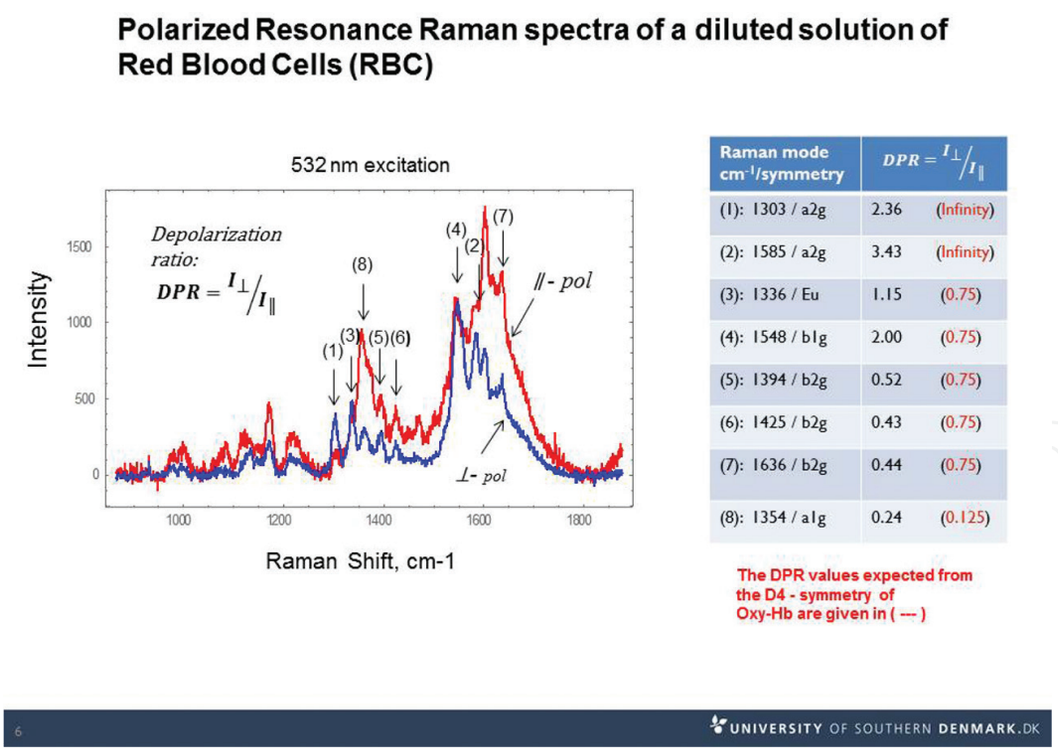

Figure 6. Left: polarized resolved, fluorescence corrected RRS spectra of a diluted solution of RBCs. Right: DPR values obtained for most intense modes.

http://dx.doi.org/10.5772/65482

Figure 7 illustrates a comparison of the experimental results in **Figure 6** with simulations of the polarization dispersion curves based on the molecular H-type dimer model shown in **Figure 4**. The particular shape of the dispersion curves clearly illustrate that they depend strongly on the nature of the Raman modes. It should be noticed the simulations are based on only one adjustable parameter. The remaining parameters are estimated from Raman and other experiments.

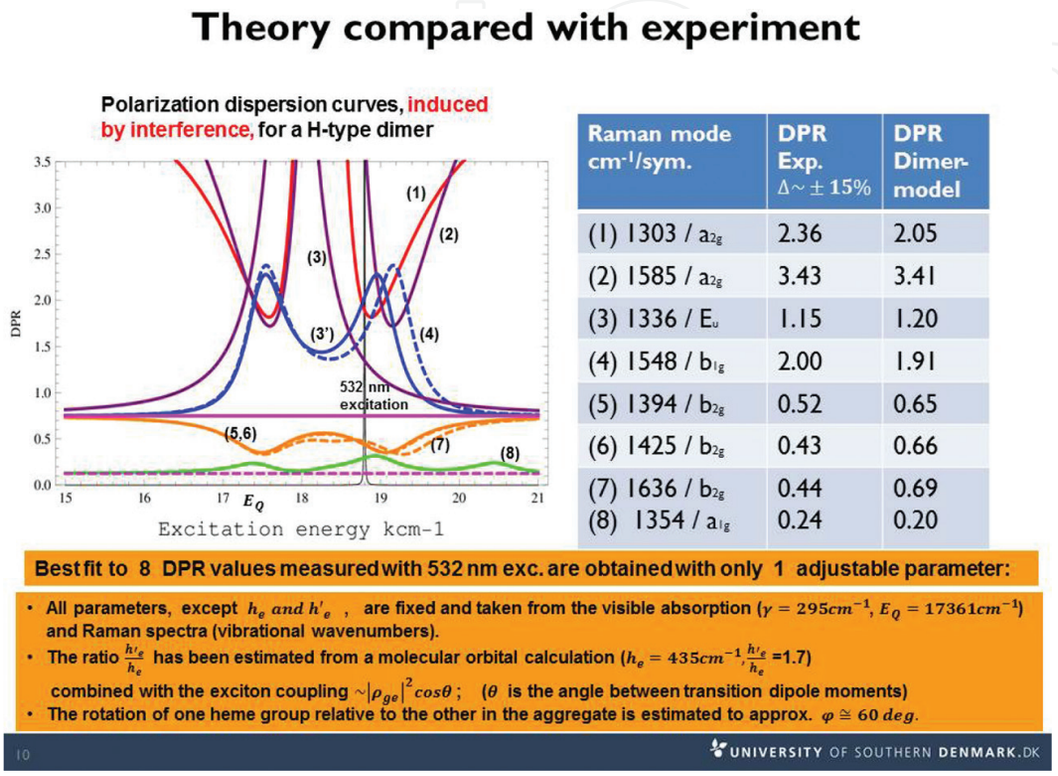

Figure 7. Theoretical interpretation of the experimental results in **Figure 6** based on a H-type dimer model.

2.2.1.1. Conclusion of case study 1

The polarized resolved RRS study of the RBC demonstrates that aggregation between the haem-protein molecules inside the RBCs can be studied *in vivo*, which, e.g. opens for the possibility of monitoring the effects of drugs added to the blood. It should be noticed that the method applies to aggregation of symmetric molecules in general.

2.2.2. Case study 2: in vitro, polarization resolved RRS study of dye-sensitized solar cells (DSC)

The basis for the polarization resolved RRS study of aggregation illustrated in Case study 1 is the observation that the DPR is very sensitive to changes in the structure of the state tensors, i.e. the number of components and the numerical relations between these. As demonstrated these changes were induced by the excitonic coupling (i.e. weak coupling) between the isolated molecules.

In the present case study, it is demonstrated that it is possible to discriminate between very similar molecules (i.e. molecules where the unpolarized Raman spectra are almost identical) by utilizing a combination of the polarization dispersion of Raman modes with a small spectral change in the visible absorption spectra. The dye-sensitized solar cells (DSC) is an illustrative example, but the method has general applicability. The idea is quite simple; the resonance condition for a given molecule depends on the wavenumber difference between the electronic absorption and the laser. Due to the spectral shift in the absorption the dispersion curve for a dispersive Raman mode will be displaced so that the excitation will 'hit' a different point on the dispersion curve. The shift in the DPR value measured at the wavenumber of the laser will depend on the nature of the dispersion (see, e.g. **Figure 5(a)** or **7**), the magnitude of spectral shift in the absorption and of the wavenumber of the laser chosen for the excitation.

When the molecules have low or no symmetry most Raman modes will in general be dispersive. When the molecular symmetry is higher the numerical relations between some of tensor elements will limit the number of dispersive modes, like in the haem-protein case, where the ideal symmetry of the chromophore (haem) is D_{4h}. However, as already emphasized the real symmetry for most proteins is lowered due to perturbations of the haem-group, with the result that several modes exhibit dispersion. Thus in reality, dispersive Raman modes are quite common.

As said, the DSCs will be considered as an example. The discussion is based on the studies performed by Hassing et al. in [31, 32], in which the stability of the Ruthenium-based dye (N719) and the properties of dye-sensitized solar cells (DSC) based on N719 was studied by polarization resolved RRS. Reference to these papers is made for details and for references to the special literature on DSCs.

The working efficiency of a DSC depends on essentially of two parameters: The long-term stability of the dye itself and on the microscopic structure of the dye-semiconductor interface (N719-TiO_2). Raman spectroscopy is an attractive technique for on-site investigations of DSCs, since no sample preparations are required, the measurements can be performed through the cover glass of the DSC and Raman spectra have in general a high molecular specificity. The chemical structure of N719 and of its main degradation product N719-TBP is shown in **Figure 1** in [32]. In the investigations of the dye stability one must be able to discriminate between these molecules. The unpolarized RRS spectra measured on solutions of N719 and N719-TBP [31] show that the spectra are nearly identical with respect to the main spectroscopic features, which might lead to the conclusion that N719 has not degraded. The unpolarized RRS spectra obtained from DSC samples fabricated with a different relative amount of N719 and N719-TBP gives the same result for the prominent and well-defined spectral features. Although certain spectral changes are found these are small and only related to the Raman bands with very low intensity [33]. Another issue in the RRS investigation of the performance of the DSC is to estimate the relative amount of N719 molecules adsorbed to the surface of the TiO_2 semiconductor and as compared to those which are desorbed, see [34]. The measured unpolarized RRS spectra originate from a mixture of adsorbed and desorbed N719 molecules. These spectra cannot be discriminated since both the spectra of the adsorbed and desorbed molecules are approximately equally resonance enhanced (see **Figure 8**) and besides similar. The same situation holds for the N719-TBP molecules.

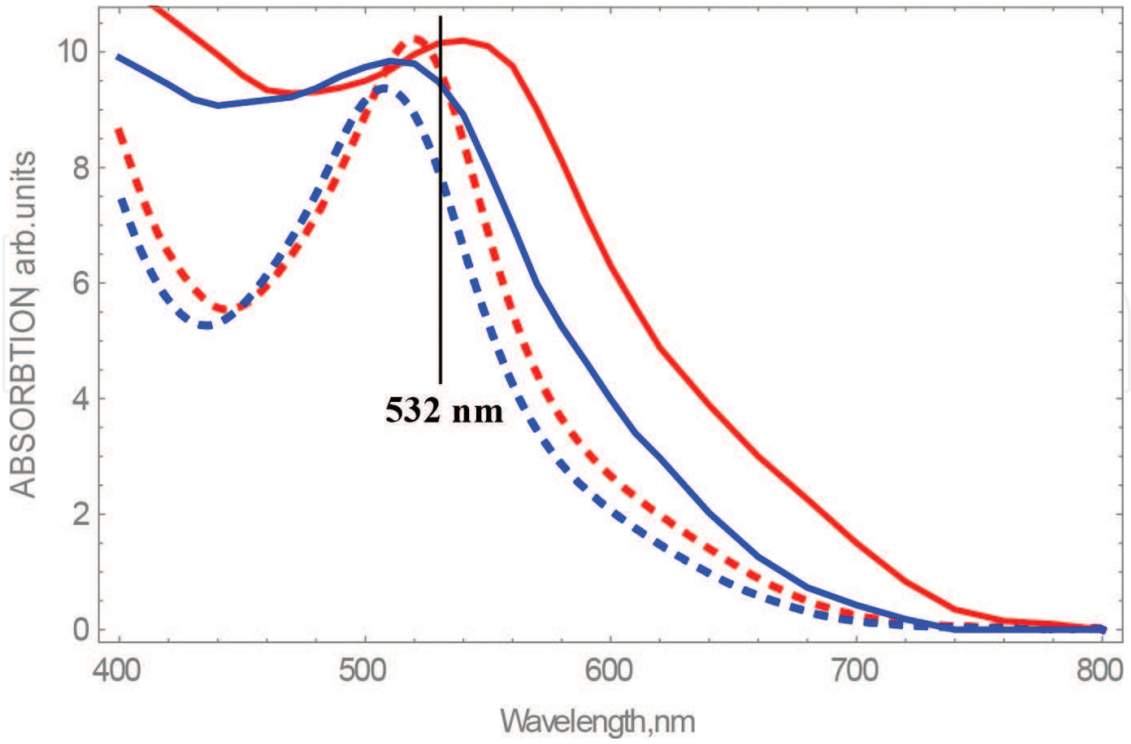

Figure 8. Visible absorption spectra of $DSC_{100/0}$ (solid red), $DSC_{0/100}$ (solid blue), N719 in methanol (dashed red) and N719-TBP in methanol (dashed blue). Laser wavelength for RRS is 532 nm. The spectral shifts between the spectra are in the region 13–30 nm.

Figure 8 shows the visible absorption spectra of DSC samples with 100% N719 ($DSC_{100/0}$), 100% N719-TBP ($DSC_{0/100}$) and solutions of N719 and N719-TBP.

The DPR values obtained from the polarization resolved and fluorescence subtracted RRS spectra for the solutions of N719 and N719-TBP in methanol and for the DSC-samples $DSC_{100/0}$ and $DSC_{0/100}$ have been collected in **Figure 9** for comparison.

It follows from **Figure 9** that although the positions of the Raman bands are almost the same for the four molecules considered (the shifts in band positions lie between 0 and 2 cm^{-1}) most of the DPR values will change when comparing either the values for the solutions of N719 and N719-TBP or the values for the DSC-samples $DSC_{100/0}$ and $DSC_{0/100}$. The observed shifts in the DPR values originate from the combined effect of the spectral shift in the electronic absorption spectra (e.g. ~13mm for the solutions) and the fact that the modes are dispersive. Since the observed changes in most DPR values are significant and also related to the most intense Raman bands, the polarized resolved RRS has a larger potential for monitoring the stability than the unpolarized RRS, where the conclusions have to rely on small spectral changes in bands with low signal-to-noise (S/N) ratio.

However, the most striking result reflected in **Figure 9** is the large change in the DPR values observed between adsorbed and non-adsorbed N719 molecules and/or between adsorbed and non-adsorbed N719-TBP molecules.

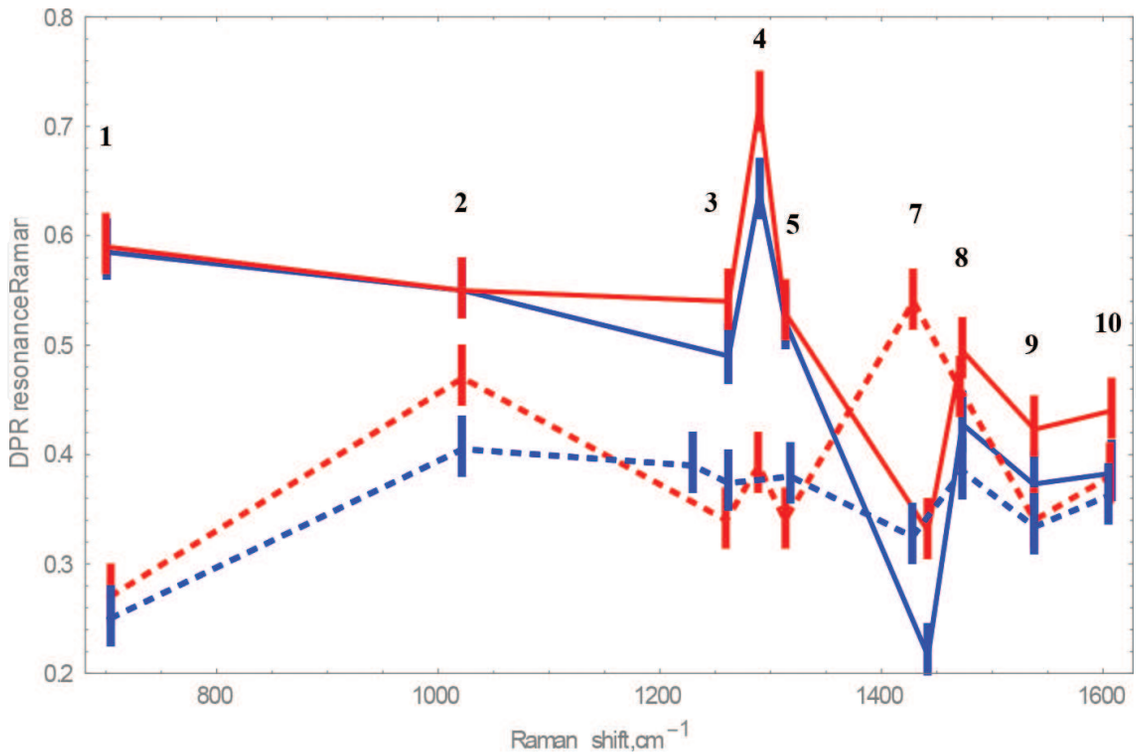

Figure 9. DPR values and estimated uncertainty ±0.025 for the DSC samples: $DSC_{100,0}$ (solid, red) and $DSC_{0,100}$ (solid, blue), for the solutions of N719 (dashed, red) and N719-TBP (dashed, blue) for the most prominent Raman bands 1–10, see Ref. [32] for details.

The explaination for this is probably that while the non-adsorbed molecules are randomly oriented, the molecules adsorbed to the TiO_2 surface are partially oriented. Thus, the scattering conditions for the Raman processes in the two situations are very different. From the theoretical section it follows that the polarized Raman signals (and the DPR) obtained from an oriented molecule are determined by the absolute square of those components of the Raman tensor that are selected by the molecular orientation in the coordinate system defined by the laser polarization and the polarization analyzers. For randomly oriented molecules the polarized Raman signals (and the DPR) are determined by the rotational invariants of the Raman tensor. The change in the DPR values between the adsorbed and non-adsorbed molecules that reflects both the molecular orientation and the wavenumber of the absorption spectra are changed. The large average increase of the DPR values, observed e.g. for the $DSC_{100/0}$ relative to the N719 in solution, is probably due to the partial orientation exhibited by the N719 molecules, when they are adsorbed to the TiO_2. The similarity between the DPR-graphs for the DSCs and the solutions shows that these variations are essentially due to the shifts in the absorption spectra combined with the dispersive property of the individual Raman modes. Finally, since we observe very small wavenumber shifts (0–2 cm^{-1}) in the Raman spectra for the resonance-enhanced Raman modes the nature of these modes must be similar for adsorbed and non-adsorbed molecules.

The average orientation of the adsorbed molecules depends on the physical details of the adsorption process and on the spatial structure of the TiO_2 substrate. Since for oriented molecules the DPR is determined essentially by the ratio between the absolute square of those components of the Raman tensor, which are selected by the molecular orientation, it seems

http://dx.doi.org/10.5772/65482

that more information about the adsorption process can be extracted from an extended analysis, involving the design of polarization resolved RRS experiments with this in mind.

3. Concluding remarks and challenges

As shown, the reliability as well as the kind and amount of molecular information can be improved by extending a Raman analysis to include polarization resolved experiments. For example in the studies of DSCs in [33] the spectral distribution of the strongest Raman bands in fresh and aged DSCs was found to be practically identical, while significant changes of the DPR ratios were observed in [32]. Thus, the conclusions about dye stability become more reliable, when the polarization is measured. Furthermore, the possibility for studying the adsorption-desorption at the Dye-TiO_2 interface seems promising. The polarized RBC study demonstrated that aggregation between the haem molecules inside the RBCs can be studied *in vivo*, which, e.g. opens for the possibility of monitoring the effects of drugs added to the blood. Recently, Jernshøj et al. applied a combination of dynamic light-scattering and polarization resolved RRS to study, among other things, the aggregation versus pH of Arenicola Marina extracellular haemoglobin (a giant molecule with mass **~3.6 10^6 Da** and 144 oxygen binding sites) [30]. This study demonstrates the high applicability of polarized resolved RRS with respect to extracting rather detailed information about molecular systems involving very large molecules.

Finally, three challenges that one has to face when applying polarization resolved RRS should be mentioned:

(1) *Simultaneous measurements of perpendicular and parallel polarized RRS components are mandatory*.

(2) *The determination of the depolarization ratios is sensitive to fluorescence background subtraction*.

(3) *Deconvolution of 'crowded' Raman spectra is not trivial*.

Since CCD-cameras are applied in Raman microscopes, it is in fact possible through a modification of the collection optics to monitor the parallel and perpendicular polarized spectra simultaneously. This has three important implications: the accuracy of the measured DPR is improved, since modifications of the sample induced by the laser appear in both signals, the S/N ratio can be increased through averaging a large amount of spectra and most importantly it open for performing polarized resolved Raman imaging.

Author details

Søren Hassing

Address all correspondence to: sh@kbm.sdu.dk

Institute of Chemical Engineering, Biotechnology and Environmental Technology, University of Southern Denmark, Odense M, Denmark

References

[1] Placzek G; in Handbuch der Radiologie, Ed.: Marx E, Leipzig, 1934, 2, 209–374, Akademische Verlagsgesellschaft.

[2] Sonnich Mortensen O; Raman Dispersion Spectroscopy (RADIS). J.Raman Spectrosc., 1981, 11, 329–333.

[3] Hedegaard M; Hassing S; Application of Raman dispersion spectroscopy in 3-way multivariate data analysis. J.Raman spectrosc. 2008, 39(4), 478–489.

[4] Lemke C; Dreybrodt W; Shelnutt J; Quirke J M E.; Schweitzer-Stenner R; Polarized Raman Dispersion Spectroscopy probes planar and non-planar distortions ofNi(II)-porphyrins with different peripheral substituents. J. Raman Spectrosc., 1998, 29, 945–953.

[5] Nagar S; Schweitzer-Stenner R; Dreybrodt W; Mayer A; Determination of the Raman Tensor of the Haem Group in Myoglobin by Resonance Raman Scattering in Solution and Single Crystals. Biophys Struct Mech, 1984, 10, 257–273.

[6] Bobinger U; Schweitzer-Stenner R; Dreybrodt W; Highly resolved depolarization dispersion and excitation profiles of Raman fundamentals of protoporphyrin IX in a cytochrome c matrix. J.Raman Spectrosc.1989, 20, 191–202

[7] Schweitzer-Stenner R; Wedekind D; Dreybrodt W; Detection of heme perturbations caused by the quaternary R->T transition in oxyhemoglobin trout IV by resonance Raman scattering. Biophys. J. 1989,55, 703–712.

[8] Long D A; The Raman Effect; John Wiley & Sons, Chichester (UK), 2002.

[9] Mortensen O S; Hassing S; Polarization and Interference Phenomena in resonance Raman scattering; In: Clarke R J H, Hester R E , editors. Advances in Infrared and Raman Spectroscopy, Vol. 6, Chapter 1, Wiley, New York (US) , 1980.

[10] Siebrand W; Zgierski M Z; In: Lim C; editor, Excited States Vol. 4, 1–134, Academic Press. Inc. New York, 1979.

[11] Long D A; Raman Spectroscopy, McGraw Hill, London UK, 1977

[12] Schweitzer-Stenner R; Polarized Resonance Raman Dispersion Spectroscopy on Metalporphyrins. J. Porphyr. Phthal. 5, 198–224, 2001.

[13] Sonnich Mortensen O; In: Structure and Bonding 69, 1–38; Springer-Verlag, 1987.

[14] Schweitzer-Stenner R; Bosenbeck M; Dreybrodt W; Raman dispersion spectroscopy probes heme distortions in deoxy-Hb trout IV involved in its T-state Bohr-effect. Biophysical Journal, 1993, 64, 1194–1209.

[15] Kelley A M; A multimode vibronic treatment of absorption, resonance Raman, and hyper-Rayleigh scattering of excitonically coupled molecular dimers. J. Chem Phys, 2003, 119(6), 3320–3331.

[16] Wood B R; McNaughton D; Resonance Raman spectroscopy in malaria research. Expert Rev. Proteomics, 2006, 3(5), 525–544.

[17] Frosch T; Koncarevic S; Becker K; Popp J; Morphology-sensitive Raman modes of the malaria pigment hemozoin. Analyst, 2009, 134,1126–1132.

[18] Shelnutt J A; Cheung L D; Chang R C C; Yu N; Felton, L H; Resonance Raman spectra of metalloporphyrins. Effects of Jahn-Teller instability and nuclear distortion on excitation profiles of Stokes fundamentals. J. Chem. Phys., 1977, 66, 3387–3398.

[19] Shelnutt J A; O'Shea D C; Resonance Raman spectra of copper tetraphenylporphyrin: Effects of strong vibronic coupling on excitation profiles and the absorption spectrum. J. Chem. Phys., 1978, 69, 5361–5374.

[20] Zgierski M Z; Pawlikowski M; Chemical Physics 1982, 65, 335–367.

[21] Schweitzer-Stenner R; Revisited Depolarization Ratio Dispersion of Raman Fundamentals from Heme c in Ferrocytochrome c Confirms That Asymmetric Perturbations Affect the Electronic and Vibrational Structure of the Chromophore's Macrocycle. J. Phys. Chem., 1994, 98, 9374–9379.

[22] Huang G; Szigeti K; Fidy J; Schweitzer-Stenner R; Structural Disorder of Native Horseradish Peroxidase C probed by Resonance Raman and Low Temperature Optical Absorption spectroscopy. J.Phys.Chem. B, 2003, 107,2822–2830.

[23] Jentzen M; Ma J; Shelnutt J A; Conservation of the Conformation of the Porphyrin Macrocycle in Hemoproteins Biophysical Journal, 1998, 74,753–763.

[24] Haddad R E; Gazeau S; P′ecaut J; Marchon J; Medforth C J; Craig J; Shelnutt J A. Origin of the Red Shifts in the Optical Absorption Bands of Nonplanar Tetraalkylporphyrins. J. Am. Chem. Soc., 2003, 125, 1253–1268.

[25] Xu L; Li Z; Tan W; He T; Liu F; Chen D; Density functional theory studies on the Raman and IR spectra of *meso*-tetraphenylporphyrin diacid. Spectrochimica Acta Part A, 2005, 62, 850–862.

[26] Ma Y P; He S G; Ding X L; Wang Z C; Xue W; Shi Q; Theoretical study of intermolecular interactions in meso-tetraphenylporphyrin diacid dimer (H4TPPCl2)2 . Physical Chemistry Chemical Physics, 2009, 11, 2543–2552

[27] Wood B R; McNaughton D; Raman excitation wavelength investigation of single red blood cells in vivo. J. Raman Spectrosc., 2002, 33, 517–523.

[28] Ramser K; Logg K; Goksör M; Enger J; Käll M; Hanstorp D; Resonance Raman spectroscopy of optically trapped functional erythrocytes. Journal of Biomedical Optics, 2004, 9(3), 593–600.

[29] Wood B R; Hammer L; McNaughton D; Resonance Raman spectroscopy provides evidence of heme ordering within the functional erythrocyte. Vibrational Spectroscopy, 2005, 38, 71–78.

[30] Jernshøj K D; Hassing S; Olsen L F; A combination of dynamic light scattering and polarized resonance Raman scattering applied in the study of Arenicola Marina extracellular hemoglobin. J Chem Phys, 2013, 139 (6), 065104–1–10.

[31] Hassing S; Jernshøj K D; Nguyen P T; Lund T; J. Investigation of the Stability of the Ruthenium-Based Dye (N719) Utililizing the Polarization Properties of Dispersive Raman Modes and/or of the Fluorescent Emission. J. Physical Chemistry C, 2013, 117, 23500–23506.

[32] Hassing S; Jernshøj K D; Nguyen P T; Lund T; In Vitro Polarized Resonance Raman Study of N719 and N719-TBP in Dye Sensitized Solar Cells. J. Technology Innovations in Renewable Energy, 2016, 5, 21–32.

[33] Likodimos V; Stergiopoulos T; Falaras P; Hariksun R; Desilvestro J; Tulloch, G; Prolonged Light and Thermal Stress Effects on Industrial Dye-Sensitized Solar Cells: A Micro-Raman Investigation on the Long-Term Stability of Aged Cells. J. Phys. Chem. C 2009; 113, 9412–9422.

[34] Perez Leon C; Kador L; Peng B; Thelakkat M; Characterization of the Adsorption of Ru-bpy Dyes on Mesoporous TiO2 Films with UV-Vis, Raman and FTIR Spectroscopy. J. Chem. Phys. B, 2006, 110 (17), 8723–8730.

IntechOpen